

Stray magnetic fields from elliptical-shaped and stadium-shaped ferromagnets

Tomohiro Taniguchi*

*National Institute of Advanced Industrial Science and Technology (AIST),
Research Center for Emerging Computing Technologies, Tsukuba 305-8568, Japan*

(Dated: October 27, 2023)

An artificial spin ice consisting of numerous ferromagnets has attracted attention because of its applicability to practical devices. The ferromagnets interact through their stray magnetic field and show various functionality. The ferromagnetic element in the spin ice was recently made in elliptical-shape or stadium-shape. The former has a narrow edge, expecting to generate a large stray magnetic field. The latter has a large volume and is also expected to generate a large stray magnetic field. Here, we estimate the stray magnetic field by numerically integrating the solution of the Poisson equation. When magnetization is parallel to an easy axis, the elliptical-shaped ferromagnet generates a larger stray magnetic field than the stadium-shaped ferromagnet. The stray magnetic fields from both ferromagnets for arbitrary magnetization directions are also investigated.

I. INTRODUCTION

Computation of magnetic field from a ferromagnetic body, or more generally solving a Poisson equation, has been an attractive problem in both mathematics and physics [1–12], and still prompts publications recently [13–18]. Even after great development of numerical solvers [19–24], deriving a solution of potential, or field, in terms of analytical functions or in forms of some integrals with simplified approximations, such as macrospin or rigid-vortex assumption, is highly demanded, particularly when many-body problems are of interest [25–29]. This is because it enables us to estimate various parameters, such as coercive and stray fields, with adequate calculation cost. The past works have mainly focused on the internal magnetic field and derived the solutions of the demagnetization coefficients for various shapes of ferromagnets such as ellipsoid, cylinder, and cuboid [1–6, 8–10], while the stray magnetic field, originated from magnetostatic interaction, for vortex, cylinder, and so on has also been investigated [7, 11–18].

An interesting target nowadays related to this is to compare stray magnetic fields from two kinds of uniformly magnetized ferromagnets, namely elliptical-shaped and stadium-shaped ferromagnets [30, 31], which are schematically shown in Figs. 1(a) and 1(b), respectively. They are recently used as a fundamental element of artificial spin ice, and their stray magnetic fields are the origin of the frustration in it through magnetostatic interaction [32–39]. The frustrated states of the ferromagnets are expected to be used in several applications such as multibit memory and neuromorphic computing [40–42]. Therefore, the evaluation and comparison from these two kinds of ferromagnets are of great interest. Let us assume that the length and width of these two ferromagnets, which are $2a$ and $2b$ in Fig. 1, are the same. Accordingly, the stadium-shaped ferromagnet has a larger volume compared with the elliptical-shaped ferromagnet. From this perspective, the stadium-shaped

ferromagnet is expected to generate a larger stray magnetic field. However, we should note that the magnetic pole of the elliptical-shaped ferromagnet is concentrated in a narrower region (around $x \simeq \pm a$ in Fig. 1) compared with that in the stadium-shaped ferromagnet, when the magnetization points parallel to the easy (long) axis. In this sense, the elliptical-shaped ferromagnet is expected to generate a larger stray field. Then, a question arises as to which shape of the ferromagnet generates a larger stray field. Here, we compute their stray magnetic fields with macrospin assumption and study this question. Starting from Maxwell equations in a steady state, $\nabla \cdot \mathbf{B} = 0$ and $\nabla \times \mathbf{H} = \mathbf{0}$, where \mathbf{B} and \mathbf{H} are the magnetic flux density and the magnetic field, respectively, the magnetic potential V , satisfying $\mathbf{H} = -\nabla V$, obeys $\nabla^2 V = 4\pi \nabla \cdot \mathbf{M}$, where \mathbf{M} is the magnetization. The solution of this Poisson equation is

$$V(\mathbf{r}) = \oint dS' \frac{\mathbf{n} \cdot \mathbf{M}}{|\mathbf{r} - \mathbf{r}'|}, \quad (1)$$

where dS is an infinitesimal cross-section area of the integral region, while \mathbf{n} is a unit vector orthogonal to the surface dS . The stray magnetic field is estimated from Eq. (1) as $\mathbf{H} = -\nabla V$. It is found that the elliptical-shaped ferromagnet generates a larger stray magnetic field along the direction of the easy axis while the stadium-shaped ferromagnet generates a larger stray magnetic field along the in-plane hard-axis direction.

II. STRAY FIELD FROM AN ELLIPTICAL-SHAPED FERROMAGNET

Here, we derive a formula of the stray magnetic field from an elliptical-shaped ferromagnet. The geometry is schematically shown in Fig. 2(a). In the following, we denote that magnetization direction in terms of the zenith and azimuth angles, θ and φ , as $\mathbf{M} = M(\sin \theta \cos \varphi, \sin \theta \sin \varphi, \cos \theta)$. Since the Poisson equation is a linear equation, its solution is a superposition of the solutions, where the magnetization points to in-plane (xy -plane) and perpendicular (z -axis) directions.

* tomohiro-taniguchi@aist.go.jp

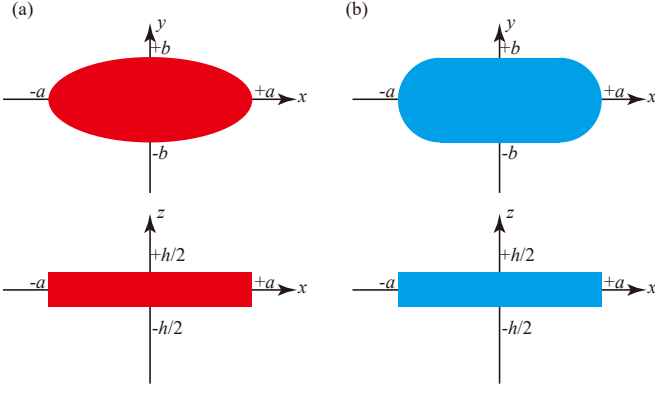


FIG. 1. (Color online) Top and side views of (a) elliptical-shaped and (b) stadium-shaped ferromagnets. The length in the long-axis (x -axis) direction and the width in the short-axis (y -axis) direction are $2a$ and $2b$, respectively, while the height in the z direction is h .

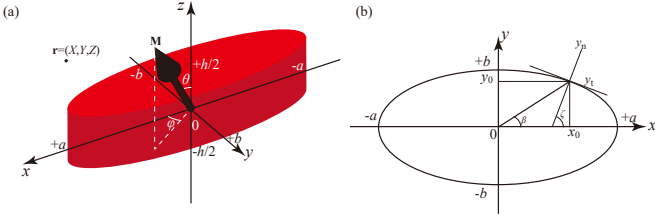


FIG. 2. (Color online) (a) Bird's eye view of the elliptical-shaped ferromagnet. (b) Top view of the elliptical-shaped ferromagnet, where the tangent y_t and normal y_n with at a point (x_0, y_0) , as well as the angles β and ζ , are indicated.

Therefore, we denote the solution of the magnetic potential V for the in-plane and perpendicularly magnetized ferromagnets as V_i and V_p , respectively. The measurement point of the potential is $\mathbf{r} = (X, Y, Z)$. The magnetic field at this point is $\mathbf{H}(\mathbf{r}) = -\nabla V|_{\mathbf{x}=\mathbf{r}} = (-\partial V/\partial x, -\partial V/\partial y, -\partial V/\partial z)_{\mathbf{x}=\mathbf{r}}$.

A. Magnetic potential

To derive the solution of V for the elliptical-shaped ferromagnet, it is useful to introduce an elliptic coordinate, where the positions x and y in the Cartesian coordinate are related to new variables, α and β , as $x = c \cosh \alpha \cos \beta$ and $y = c \sinh \alpha \sin \beta$, where $-\infty \leq \alpha \leq \infty$ and $-\pi \leq \beta \leq \pi$, while $c = \sqrt{a^2 - b^2}$. We also introduce

$$\alpha_e = \frac{1}{2} \ln \left(\frac{a+b}{a-b} \right). \quad (2)$$

Let us denote a point on the circumference of the ellipse as (x_0, y_0) ; see also Fig. 2(b). The tangent and normal with respect to the point are, respectively, given by

$$y_t = \frac{b^2}{a^2} \left(1 - \frac{x_0}{a} \right), \quad (3)$$

$$y_n = \frac{a^2 y_0}{b^2 x_0} - y_0 \left(\frac{a^2}{b^2} - 1 \right). \quad (4)$$

The angle ζ between y_n and the x -axis satisfies

$$\cos \zeta = \frac{b^2 \cosh \alpha_e \cos \beta}{\sqrt{b^4 \cosh^2 \alpha_e \cos^2 \beta + a^4 \sinh^2 \alpha_e \sin^2 \beta}}, \quad (5)$$

$$\sin \zeta = \frac{a^2 \sinh \alpha_e \sin \beta}{\sqrt{b^4 \cosh^2 \alpha_e \cos^2 \beta + a^4 \sinh^2 \alpha_e \sin^2 \beta}}. \quad (6)$$

Therefore, the projection of the magnetization to the normal vector, $\mathbf{n} \cdot \mathbf{M}$, becomes $M_n = M \sin \theta (\cos \varphi \cos \zeta + \sin \varphi \sin \zeta)$. An infinitesimal cross-section area around the point (x_0, y_0) is a product of infinitesimal lines in the xy -plane, $\sqrt{x_0^2 + y_0^2} d\beta$, and along the z -direction, dz , as $dS = \sqrt{x_0^2 + y_0^2} d\beta dz = c \sqrt{\cosh^2 \alpha_e \cos^2 \beta + \sinh^2 \alpha_e \sin^2 \beta} d\beta dz$. Accordingly, the magnetic potential V_i generated from the in-plane magnetized elliptical-shaped ferromagnet becomes

$$V_i = M \sin \theta \int_{-h/2}^{h/2} dz' \int_{-\pi}^{\pi} d\beta \frac{c \sqrt{\cosh^2 \alpha_e \cos^2 \beta + \sinh^2 \alpha_e \sin^2 \beta}}{\sqrt{(x - c \cosh \alpha_e \cos \beta)^2 + (y - c \sinh \alpha_e \sin \beta)^2 + (z - z')^2}} \times \left(\frac{b^2 \cosh \alpha_e \cos \beta \cos \varphi + a^2 \sinh \alpha_e \sin \beta \sin \varphi}{\sqrt{b^4 \cosh^2 \alpha_e \cos^2 \beta + a^4 \sinh^2 \alpha_e \sin^2 \beta}} \right). \quad (7)$$

When the magnetization points to the perpendicular (z) direction, the infinitesimal cross-section area is $dx dy = J d\alpha d\beta$, where the Jacobian J is $(c^2/2)(\cosh 2\alpha - \cos 2\beta)$. Note that there are two magnetic poles, $\mathbf{n} \cdot \mathbf{M}$,

appearing on the xy -planes at $z = h/2$ and $z = -h/2$, with the opposite sign. Thus, the magnetic potential V_p generated from the perpendicularly magnetized elliptical-shaped ferromagnet is

$$V_p = M \cos \theta \int_0^{\alpha_e} d\alpha \int_{-\pi}^{\pi} d\beta \frac{c^2 (\cosh 2\alpha - \cos 2\beta)}{2} \left[\frac{1}{\sqrt{(x - c \cosh \alpha \cos \beta)^2 + (y - c \sinh \alpha \sin \beta)^2 + (z - h/2)^2}} - \frac{1}{\sqrt{(x - c \cosh \alpha \cos \beta)^2 + (y - c \sinh \alpha \sin \beta)^2 + (z + h/2)^2}} \right]. \quad (8)$$

B. Magnetic field

The x , y , and z components of the magnetic field are given by

$$H_x = M \sin \theta \int_{-h/2}^{h/2} dz' \int_{-\pi}^{\pi} d\beta \frac{c \sqrt{\cosh^2 \alpha_e \cos^2 \beta + \sinh^2 \alpha_e \sin^2 \beta} (x - c \cosh \alpha_e \cos \beta)}{[(x - c \cosh \alpha_e \cos \beta)^2 + (y - c \sinh \alpha_e \sin \beta)^2 + (z - z')^2]^{3/2}} \times \left(\frac{b^2 \cosh \alpha_e \cos \beta \cos \varphi + a^2 \sinh \alpha_e \sin \beta \sin \varphi}{\sqrt{b^4 \cosh^2 \alpha_e \cos^2 \beta + a^4 \sinh^2 \alpha_e \sin^2 \beta}} \right) + M \cos \theta \int_0^{\alpha_e} d\alpha \int_{-\pi}^{\pi} d\beta \frac{c^2 (\cosh 2\alpha - \cos 2\beta)}{2} (x - c \cosh \alpha \cos \beta) \times \left[\frac{1}{[(x - c \cosh \alpha \cos \beta)^2 + (y - c \sinh \alpha \sin \beta)^2 + (z - h/2)^2]^{3/2}} - \frac{1}{[(x - c \cosh \alpha \cos \beta)^2 + (y - c \sinh \alpha \sin \beta)^2 + (z + h/2)^2]^{3/2}} \right], \quad (9)$$

$$H_y = M \sin \theta \int_{-h/2}^{h/2} dz' \int_{-\pi}^{\pi} d\beta \frac{c \sqrt{\cosh^2 \alpha_e \cos^2 \beta + \sinh^2 \alpha_e \sin^2 \beta} (y - c \sinh \alpha_e \sin \beta)}{[(x - c \cosh \alpha_e \cos \beta)^2 + (y - c \sinh \alpha_e \sin \beta)^2 + (z - z')^2]^{3/2}} \times \left(\frac{b^2 \cosh \alpha_e \cos \beta \cos \varphi + a^2 \sinh \alpha_e \sin \beta \sin \varphi}{\sqrt{b^4 \cosh^2 \alpha_e \cos^2 \beta + a^4 \sinh^2 \alpha_e \sin^2 \beta}} \right) + M \cos \theta \int_0^{\alpha_e} d\alpha \int_{-\pi}^{\pi} d\beta \frac{c^2 (\cosh 2\alpha - \cos 2\beta)}{2} (y - c \sinh \alpha \sin \beta) \times \left[\frac{1}{[(x - c \cosh \alpha \cos \beta)^2 + (y - c \sinh \alpha \sin \beta)^2 + (z - h/2)^2]^{3/2}} - \frac{1}{[(x - c \cosh \alpha \cos \beta)^2 + (y - c \sinh \alpha \sin \beta)^2 + (z + h/2)^2]^{3/2}} \right], \quad (10)$$

$$H_z = M \sin \theta \int_{-h/2}^{h/2} dz' \int_{-\pi}^{\pi} d\beta \frac{c \sqrt{\cosh^2 \alpha_e \cos^2 \beta + \sinh^2 \alpha_e \sin^2 \beta} (z - z')}{[(x - c \cosh \alpha_e \cos \beta)^2 + (y - c \sinh \alpha_e \sin \beta)^2 + (z - z')^2]^{3/2}} \times \left(\frac{b^2 \cosh \alpha_e \cos \beta \cos \varphi + a^2 \sinh \alpha_e \sin \beta \sin \varphi}{\sqrt{b^4 \cosh^2 \alpha_e \cos^2 \beta + a^4 \sinh^2 \alpha_e \sin^2 \beta}} \right) + M \cos \theta \int_0^{\alpha_e} d\alpha \int_{-\pi}^{\pi} d\beta \frac{c^2 (\cosh 2\alpha - \cos 2\beta)}{2} \times \left[\frac{z - h/2}{[(x - c \cosh \alpha \cos \beta)^2 + (y - c \sinh \alpha \sin \beta)^2 + (z - h/2)^2]^{3/2}} - \frac{z + h/2}{[(x - c \cosh \alpha \cos \beta)^2 + (y - c \sinh \alpha \sin \beta)^2 + (z + h/2)^2]^{3/2}} \right]. \quad (11)$$

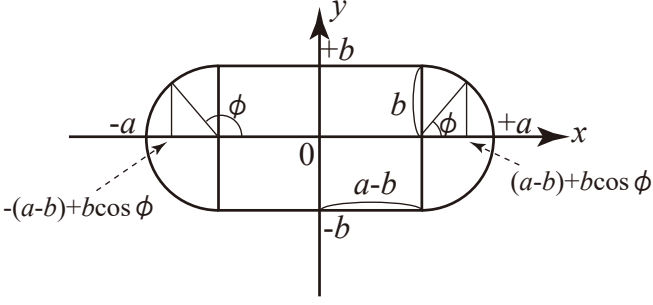


FIG. 3. (Color online) Top view of the stadium-shaped ferromagnet, which can be regarded as a cylinder with a radius b separated by a cuboid at the center. Definition of ϕ of the cylinder coordinate is also shown. The value of the x coordinate of a point on the circumference is $\pm(a-b) + b \cos \phi$.

III. STRAY FIELD FROM A STADIUM-SHAPED FERROMAGNET

Here, we derive a formula of the stray magnetic field from a stadium-shaped ferromagnet. We note that the stadium-shaped ferromagnet can be regarded as a cylinder ferromagnet with a radius b and height h , which is

separated by a cuboid with a long side $2(a-b)$, short side $2b$, and height h ; see Fig. 3. Accordingly, the stray magnetic field of this ferromagnet can be obtained as a superposition of the stray magnetic fields from cylinder-shaped and cuboid-shaped ferromagnets. The magnetic fields generated by these ferromagnets can be expressed in terms of analytical and special functions, as shown in Supplementary Material of Ref. [13]. We keep, however, integral forms of the magnetic field because the expression of the field by these functions will be greatly complex.

A. Stray magnetic field generated by magnetization pointing in x direction

Let us first consider a case where the magnetization \mathbf{M} points to the x direction. The magnetic pole, $\mathbf{n} \cdot \mathbf{M}$, in this case appears only in the side of the cylinder parts. Thus, it is convenient to introduce a cylinder coordinate (ρ, ϕ, z) , which relates to the Cartesian coordinate as $x = \rho \cos \phi$ and $y = \rho \sin \phi$. An infinitesimal cross-section area on the side of the cylinder is $b d\phi dz$, while the magnetic pole $\mathbf{n} \cdot \mathbf{M}$ on this area is $M \cos \phi$. Therefore, the magnetic potential is given by (see also Fig. 3)

$$V_{i,x} = M \int_{-\pi/2}^{\pi/2} d\phi \int_{-h/2}^{h/2} dz' \frac{b \cos \phi}{\sqrt{[x - (a-b) - b \cos \phi]^2 + (y - b \sin \phi)^2 + (z - z')^2}} + M \int_{\pi/2}^{3\pi/2} d\phi \int_{-h/2}^{h/2} dz' \frac{b \cos \phi}{\sqrt{[x + (a-b) - b \cos \phi]^2 + (y - b \sin \phi)^2 + (z - z')^2}}, \quad (12)$$

or by redefining ϕ in the second integral as $\phi - \pi$,

$$V_{i,x} = M \int_{-\pi/2}^{\pi/2} d\phi \int_{-h/2}^{h/2} dz' \left\{ \frac{b \cos \phi}{\sqrt{[x - (a-b) - b \cos \phi]^2 + (y - b \sin \phi)^2 + (z - z')^2}} - \frac{b \cos \phi}{\sqrt{[x + (a-b) + b \cos \phi]^2 + (y + b \sin \phi)^2 + (z - z')^2}} \right\}. \quad (13)$$

The stray magnetic field $\mathbf{H} = -\nabla V_{i,x}$ is given by

$$H_{xx} = M \int_{-\pi/2}^{\pi/2} d\phi \int_{-h/2}^{h/2} dz' \left(\frac{[x - (a-b) - b \cos \phi] b \cos \phi}{\{[x - (a-b) - b \cos \phi]^2 + (y - b \sin \phi)^2 + (z - z')^2\}^{3/2}} - \frac{[x + (a-b) + b \cos \phi] b \cos \phi}{\{[x + (a-b) + b \cos \phi]^2 + (y + b \sin \phi)^2 + (z - z')^2\}^{3/2}} \right), \quad (14)$$

$$H_{yx} = M \int_{-\pi/2}^{\pi/2} d\phi \int_{-h/2}^{h/2} dz' \left(\frac{(y - b \sin \phi) b \cos \phi}{\{[x - (a - b) - b \cos \phi]^2 + (y - b \sin \phi)^2 + (z - z')^2\}^{3/2}} \right. \\ \left. - \frac{(y + b \cos \phi) b \cos \phi}{\{[x + (a - b) + b \cos \phi]^2 + (y + b \sin \phi)^2 + (z - z')^2\}^{3/2}} \right). \quad (15)$$

$$H_{zx} = M \int_{-\pi/2}^{\pi/2} d\phi \int_{-h/2}^{h/2} dz' \left(\frac{(z - z') b \cos \phi}{\{[x - (a - b) - b \cos \phi]^2 + (y - b \sin \phi)^2 + (z - z')^2\}^{3/2}} \right. \\ \left. - \frac{(z - z') b \cos \phi}{\{[x + (a - b) + b \cos \phi]^2 + (y + b \sin \phi)^2 + (z - z')^2\}^{3/2}} \right). \quad (16)$$

B. Stray magnetic field generated by magnetization pointing in y direction

Next, we calculate the stray magnetic field when the magnetization points to the y direction. The magnetic

potential in this case is the sum of those generated by the magnetic poles appear on the sides of the cylinder and cuboid. The former contribution, similar to $V_{i,x}$ is

$$V_{i,y,cy} = M \int_{-\pi/2}^{\pi/2} d\phi \int_{-h/2}^{h/2} dz' \frac{b \sin \phi}{\sqrt{[x - (a - b) - b \cos \phi]^2 + (y - b \sin \phi)^2 + (z - z')^2}} \\ + M \int_{\pi/2}^{3\pi/2} d\phi \int_{-h/2}^{h/2} dz' \frac{b \sin \phi}{\sqrt{[x + (a - b) - b \cos \phi]^2 + (y - b \sin \phi)^2 + (z - z')^2}}, \quad (17)$$

or equivalently,

$$V_{i,y,cy} = M \int_{-\pi/2}^{\pi/2} d\phi \int_{-h/2}^{h/2} dz' \left\{ \frac{b \sin \phi}{\sqrt{[x - (a - b) - b \cos \phi]^2 + (y - b \sin \phi)^2 + (z - z')^2}} \right. \\ \left. - \frac{b \sin \phi}{\sqrt{[x + (a - b) + b \cos \phi]^2 + (y + b \sin \phi)^2 + (z - z')^2}} \right\}, \quad (18)$$

while the latter contribution is

$$V_{i,y,cu} = M \int_{-(a-b)}^{(a-b)} dx' \int_{-h/2}^{h/2} dz' \left[\frac{1}{\sqrt{(x - x')^2 + (y - b)^2 + (z - z')^2}} - \frac{1}{\sqrt{(x - x')^2 + (y + b)^2 + (z - z')^2}} \right]. \quad (19)$$

The stray magnetic field $\mathbf{H} = -\nabla(V_{i,y,cy} + V_{i,y,cu})$ is given by

$$H_{xy} = M \int_{-\pi/2}^{\pi/2} d\phi \int_{-h/2}^{h/2} dz' \left(\frac{[x - (a - b) - b \cos \phi] b \sin \phi}{\{[x - (a - b) - b \cos \phi]^2 + (y - b \sin \phi)^2 + (z - z')^2\}^{3/2}} \right. \\ \left. - \frac{[x + (a - b) + b \cos \phi] b \sin \phi}{\{[x + (a - b) + b \cos \phi]^2 + (y + b \sin \phi)^2 + (z - z')^2\}^{3/2}} \right) \\ + M \int_{-(a-b)}^{(a-b)} dx' \int_{-h/2}^{h/2} dz' \left\{ \frac{x - x'}{[(x - x')^2 + (y - b)^2 + (z - z')^2]^{3/2}} - \frac{x - x'}{[(x - x')^2 + (y + b)^2 + (z - z')^2]^{3/2}} \right\}, \quad (20)$$

$$\begin{aligned}
H_{yy} = & M \int_{-\pi/2}^{\pi/2} d\phi \int_{-h/2}^{h/2} dz' \left(\frac{(y - b \sin \phi) b \sin \phi}{\{[x - (a - b) - b \cos \phi]^2 + (y - b \sin \phi)^2 + (z - z')^2\}^{3/2}} \right. \\
& \left. - \frac{(y + b \sin \phi) b \sin \phi}{\{[x + (a - b) + b \cos \phi]^2 + (y + b \sin \phi)^2 + (z - z')^2\}^{3/2}} \right) \\
& + M \int_{-(a-b)}^{(a-b)} dx' \int_{-h/2}^{h/2} dz' \left\{ \frac{y - b}{[(x - x')^2 + (y - b)^2 + (z - z')^2]^{3/2}} - \frac{y + b}{[(x - x')^2 + (y + b)^2 + (z - z')^2]^{3/2}} \right\}, \quad (21)
\end{aligned}$$

$$\begin{aligned}
H_{zy} = & M \int_{-\pi/2}^{\pi/2} d\phi \int_{-h/2}^{h/2} dz' \left(\frac{(z - z') b \sin \phi}{\{[x - (a - b) - b \cos \phi]^2 + (y - b \sin \phi)^2 + (z - z')^2\}^{3/2}} \right. \\
& \left. - \frac{(z - z') b \sin \phi}{\{[x + (a - b) + b \cos \phi]^2 + (y + b \sin \phi)^2 + (z - z')^2\}^{3/2}} \right) \\
& + M \int_{-(a-b)}^{(a-b)} dx' \int_{-h/2}^{h/2} dz' \left\{ \frac{z - z'}{[(x - x')^2 + (y - b)^2 + (z - z')^2]^{3/2}} - \frac{z - z'}{[(x - x')^2 + (y + b)^2 + (z - z')^2]^{3/2}} \right\}. \quad (22)
\end{aligned}$$

C. Stray magnetic field generated by magnetization pointing in z direction

Next, we calculate the stray magnetic field when the magnetization points to the z direction. The magnetic pole, $\mathbf{n} \cdot \mathbf{M}$, in this case appears on the circular and rectangular surfaces on $z = \pm h/2$ with the opposite sign. Thus, the magnetic potential is

$$\begin{aligned}
V_p = & M \int_{-\pi/2}^{\pi/2} d\phi \int_0^b \rho d\rho \left\{ \frac{1}{\sqrt{[x - (a - b) - \rho \cos \phi]^2 + (y - \rho \sin \phi)^2 + (z - h/2)^2}} \right. \\
& - \frac{1}{\sqrt{[x - (a - b) - \rho \cos \phi]^2 + (y - \rho \sin \phi)^2 + (z + h/2)^2}} \\
& + \frac{1}{\sqrt{[x + (a - b) + \rho \cos \phi]^2 + (y + \rho \sin \phi)^2 + (z - h/2)^2}} \\
& \left. - \frac{1}{\sqrt{[x + (a - b) + \rho \cos \phi]^2 + (y + \rho \sin \phi)^2 + (z + h/2)^2}} \right\} \\
& + M \int_{-(a-b)}^{(a-b)} dx' \int_{-b}^b dy' \left[\frac{1}{\sqrt{(x - x')^2 + (y - y')^2 + (z - h/2)^2}} \right. \\
& \left. - \frac{1}{\sqrt{(x - x')^2 + (y - y')^2 + (z + h/2)^2}} \right]. \quad (23)
\end{aligned}$$

Therefore, the stray magnetic field $\mathbf{H} = -\nabla V_p$ becomes

$$\begin{aligned}
H_{xz} = & M \int_{-\pi/2}^{\pi/2} d\phi \int_0^b \rho d\rho \left(\frac{x - (a - b) - \rho \cos \phi}{\{[x - (a - b) - \rho \cos \phi]^2 + (y - \rho \sin \phi)^2 + (z - h/2)^2\}^{3/2}} \right. \\
& - \frac{x - (a - b) - \rho \cos \phi}{\{[x - (a - b) - \rho \cos \phi]^2 + (y - \rho \sin \phi)^2 + (z + h/2)^2\}^{3/2}} \\
& + \frac{x + (a - b) + \rho \cos \phi}{\{[x + (a - b) + \rho \cos \phi]^2 + (y + \rho \sin \phi)^2 + (z - h/2)^2\}^{3/2}} \\
& \left. - \frac{x + (a - b) + \rho \cos \phi}{\{[x + (a - b) + \rho \cos \phi]^2 + (y + \rho \sin \phi)^2 + (z + h/2)^2\}^{3/2}} \right) \\
& + M \int_{-(a-b)}^{(a-b)} dx' \int_{-b}^b dy' \left[\frac{x - x'}{[(x - x')^2 + (y - y')^2 + (z - h/2)^2]^{3/2}} \right. \\
& \left. - \frac{x - x'}{[(x - x')^2 + (y - y')^2 + (z + h/2)^2]^{3/2}} \right], \quad (24)
\end{aligned}$$

$$\begin{aligned}
H_{yz} = & M \int_{-\pi/2}^{\pi/2} d\phi \int_0^b \rho d\rho \left(\frac{y - \rho \sin \phi}{\{[x - (a - b) - \rho \cos \phi]^2 + (y - \rho \sin \phi)^2 + (z - h/2)^2\}^{3/2}} \right. \\
& - \frac{y - \rho \sin \phi}{\{[x - (a - b) - \rho \cos \phi]^2 + (y - \rho \sin \phi)^2 + (z + h/2)^2\}^{3/2}} \\
& + \frac{y + \rho \sin \phi}{\{[x + (a - b) + \rho \cos \phi]^2 + (y + \rho \sin \phi)^2 + (z - h/2)^2\}^{3/2}} \\
& \left. - \frac{y + \rho \sin \phi}{\{[x + (a - b) + \rho \cos \phi]^2 + (y + \rho \sin \phi)^2 + (z + h/2)^2\}^{3/2}} \right) \\
& + M \int_{-(a-b)}^{(a-b)} dx' \int_{-b}^b dy' \left[\frac{y - y'}{[(x - x')^2 + (y - y')^2 + (z - h/2)^2]^{3/2}} \right. \\
& \left. - \frac{y - y'}{[(x - x')^2 + (y - y')^2 + (z + h/2)^2]^{3/2}} \right], \tag{25}
\end{aligned}$$

$$\begin{aligned}
H_{zz} = & M \int_{-\pi/2}^{\pi/2} d\phi \int_0^b \rho d\rho \left(\frac{z - h/2}{\{[x - (a - b) - \rho \cos \phi]^2 + (y - \rho \sin \phi)^2 + (z - h/2)^2\}^{3/2}} \right. \\
& - \frac{z + h/2}{\{[x - (a - b) - \rho \cos \phi]^2 + (y - \rho \sin \phi)^2 + (z + h/2)^2\}^{3/2}} \\
& + \frac{z - h/2}{\{[x + (a - b) + \rho \cos \phi]^2 + (y + \rho \sin \phi)^2 + (z - h/2)^2\}^{3/2}} \\
& \left. - \frac{z + h/2}{\{[x + (a - b) + \rho \cos \phi]^2 + (y + \rho \sin \phi)^2 + (z + h/2)^2\}^{3/2}} \right) \\
& + M \int_{-(a-b)}^{(a-b)} dx' \int_{-b}^b dy' \left[\frac{z - h/2}{[(x - x')^2 + (y - y')^2 + (z - h/2)^2]^{3/2}} \right. \\
& \left. - \frac{z + h/2}{[(x - x')^2 + (y - y')^2 + (z + h/2)^2]^{3/2}} \right]. \tag{26}
\end{aligned}$$

D. Total stray magnetic field generated from a stadium-shaped ferromagnet

Summarizing the results above, the stray magnetic field from the stadium-shaped ferromagnet, when the magnetization points to an arbitrary direction as $\mathbf{M} = M(\sin \theta \cos \varphi, \sin \theta \sin \varphi, \cos \theta)$, is

$$\mathbf{H} = \begin{pmatrix} H_{xx} & H_{xy} & H_{xz} \\ H_{yx} & H_{yy} & H_{yz} \\ H_{zx} & H_{zy} & H_{zz} \end{pmatrix} \begin{pmatrix} \sin \theta \cos \varphi \\ \sin \theta \sin \varphi \\ \cos \theta \end{pmatrix} \tag{27}$$

IV. COMPUTATION OF MAGNETIC FIELD

Here, we examine the stray magnetic fields estimated by using the above formulas. Before that, however, let us mention the validity of the above calculation briefly. We used the macrospin assumption in the derivation of the stray magnetic field. Let us also assume there is no bulk nor interfacial magnetic anisotropy. Thus, the magnetic anisotropy is solely determined by the shape magnetic anisotropy. Then, the x axis is the easy axis, while the y axis is the in-plane hard axis. We performed

micromagnetic simulation by MuMax3 [22] and found that, in the absence of an external magnetic field, the macrospin assumption works well when the magnetization points to the x direction, while it does not work for the magnetization pointing in the y direction; see Appendix. We, however, evaluate the stray magnetic field with the macrospin assumption even when the magnetization direction is not parallel to the x direction. This is because, in some practical applications such as physical reservoir computing by an artificial spin ice, a large external magnetic field is applied to the whole system [43]. In such a case, the macrospin assumption works even when the magnetization direction is deviated from the x (easy) axis; see also Appendix. Therefore, we assume in the following that an external magnetic field is applied to the x , y , or z direction to make the macrospin assumption used in the above calculations applicable. A further comparison with micromagnetic simulation is kept as a future work because it strongly depends on the system size, and its comprehensive study is beyond the scope of this work.

A. Magnetic fields when magnetization points to x , y , or z directions

Here, we show the stray magnetic fields from the elliptical-shaped and stadium-shaped ferromagnets, where the magnetization is parallel to the x , y , or z axis. The values of the parameters are $M = 1500$ emu/cm³, $a = 200$ nm, $b = 75$ nm, $h = 20$ nm [30, 31]. We compute the stray magnetic fields in a plane parallel to the xy -plane at $z = 15$ nm, which is 5 nm above the upper ferromagnetic surface at $z = +h/2 = 10$ nm.

Let us first consider the case where the magnetization is parallel to the easy (x) axis. Figures 4(a)-4(c) are the x , y , and z components of the stray magnetic fields generated from the elliptical-shaped ferromagnet, while Figs. 4(d)-4(f) show those generated from the stadium-shaped ferromagnet. Since the magnetization points to the $+x$ direction, the x component of the stray magnetic field points to the $+x$ direction for $|x| > a$, while it points to the $-x$ direction in $|x| < a$ because the magnetic field emitted near $x = +a$ returns near to $x = -a$; see Figs. 4(a) and 4(d). The y and z components of the stray magnetic fields in Figs. 4(b), 4(c), 4(e), and 4(f) can also be explained in a similar way.

Now let us remind our motivation to this study here. The stadium-shaped ferromagnet has a larger volume than the elliptical-shaped ferromagnet. In fact, their volumes are $\mathcal{V}_s = [\pi b^2 + 4b(a-b)]h$ and $\mathcal{V}_e = \pi abh$, and thus, their difference satisfies $\mathcal{V}_s - \mathcal{V}_e = (4 - \pi)b(a - b)h > 0$. Since the stray magnetic field is, roughly speaking, total number of the magnetic moments, which is the product of the magnetization and the volume, the stadium-shaped ferromagnet is expected to produce a larger stray field. The elliptical-shaped ferromagnet, however, has a narrower area near $|x| \simeq a$, and thus, the density of the magnetic pole is larger than that of the stadium-shaped ferromagnet. Therefore, it is unclear which type of the ferromagnet can generate a larger stray field. We thus evaluate the stray magnetic field along the x direction and notice that the stray magnetic fields generated from the elliptical-shaped ferromagnets are mainly larger than those generated from the stadium-shaped ferromagnet. For example, the stray magnetic field generated from the elliptical-shaped ferromagnet at $x = -300$ nm and $y = 0$ nm, i.e., 100 nm external to the ferromagnetic edge at $x = -a = -200$ nm, is 441 Oe, while that generated from the stadium-shaped ferromagnet is 281 Oe.

The situation is changed when the magnetization points to the y direction. Figures 5(a)-5(c) show the x , y , and z components of the stray magnetic field generated from the elliptical-shaped ferromagnet, where the magnetization points to the y direction. Those generated from the stadium-shaped ferromagnet is shown in Figs. 5(d)-5(f). The field distribution is, roughly speaking, rotated 90° from those shown in Fig. 4. In particular, let us focus on Figs. 5(b) and 5(e). We notice that the y component of the stray field is larger for the stadium-shaped ferromagnet than that for the elliptical-shaped

ferromagnet. For example, the stray magnetic field at $x = 0$ nm and $y = 100$ nm, i.e., 25 nm external to the ferromagnetic edge at $y = +b = 75$ nm, is 1498 Oe for the stadium-shaped ferromagnet, while that generated from the elliptical-shaped ferromagnet is 597 Oe. The large difference may arise from the difference of the ferromagnetic boundary. The magnetic field becomes large when the surface density of the magnetic pole, given by $\mathbf{M} \cdot \mathbf{n} dS$, is large. For the stadium-shaped ferromagnet, the boundary of the ferromagnet in $-(a-b) \leq x \leq +(a-b)$ is parallel to the x axis, i.e., the vector \mathbf{n} , which is normal to the area dS , is parallel to the magnetization. Thus, the density of the magnetic pole, as well as the stray magnetic field, is large. On the other hand, for the elliptical-shaped ferromagnet, the boundary is bent, and thus the vector \mathbf{n} is not parallel except at $x = 0$. Thus, the magnetic pole density, $\mathbf{M} \cdot \mathbf{n} dS$, becomes relatively small, resulting in a small stray magnetic field in the y direction.

When the magnetization points to the z direction, as shown in Fig. 6, the stray magnetic fields from the elliptical-shaped and stadium-shaped ferromagnets have similar strength, although their distributions are different depending on the sample shape.

In Fig. 7(a), the dependence of the x components of the stray magnetic fields generated from the elliptical-shaped and the stadium-shaped ferromagnets on the distance from the sample edge at $x = +a = 200$ nm are shown by the red-solid and blue-dotted lines, respectively. The y and z coordinates are 0 nm, i.e., Fig. 7(a) shows the stray magnetic field along the x axis, when the magnetization points to $+x$ direction. It is shown that the stray magnetic field generated from the elliptical-shaped ferromagnet is larger than that generated from the stadium-shaped ferromagnet, as implied from Figs. 4(a) and 4(d). Similarly, Fig. 7(b) shows the dependence of the y component of the stray magnetic field from both ferromagnets on the distance from the sample edge at $y = +b = 75$ nm, where $x = z = 0$ nm. The magnetization in this case is aligned in $+y$ direction. It can be confirmed that the stray magnetic field generated from the stadium-shaped ferromagnet is larger than that generated from the elliptical-shaped ferromagnet, as mentioned above.

In previous studies [32–38] on the artificial spin ice consisting of ferromagnets, the magnetization alignments in equilibrium were of interest, where the magnetization in each ferromagnet approximately points to the easy-axis direction, i.e., $+x$ or $-x$ direction. The frustration caused by the stray magnetic field results in a large number of degenerated ground state. It provides several interesting physical phenomena, such as residual entropy and spin liquid. The presence of a large number of the degenerated ground state is also of interest from a viewpoint of practical applications such as multibit memory and logic device [40]. In this sense, the elliptical-shaped ferromagnet will be preferable, compared with the stadium-shaped ferromagnet, because it can generate a larger stray field in the x direction and drives a strong

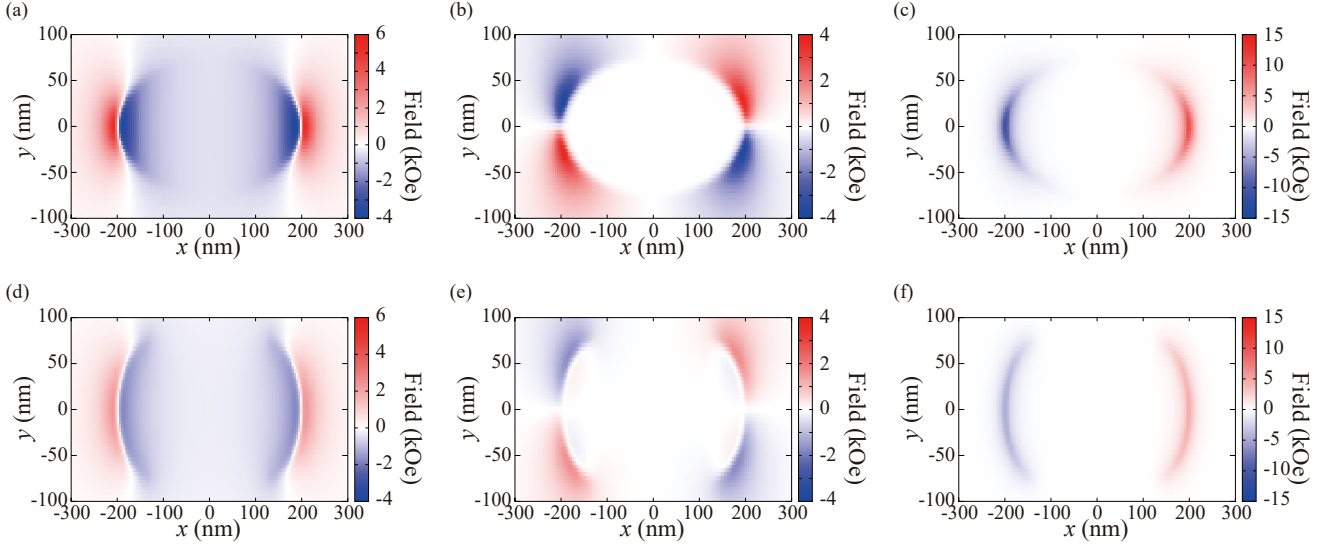


FIG. 4. (Color online) Stray fields in (a) x , (b) y , and (c) z directions generated from an elliptical-shaped ferromagnet. The magnetization points to the $+x$ direction. Those fields generated from a stadium-shaped ferromagnet are shown in (d), (e), and (f).

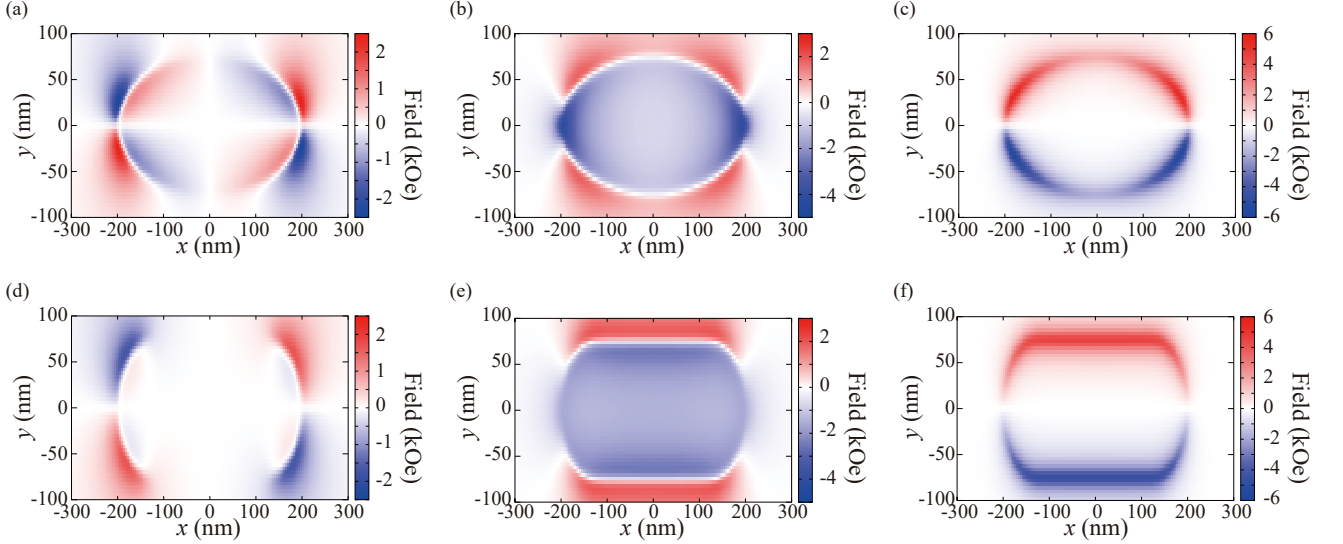


FIG. 5. (Color online) Stray fields in (a) x , (b) y , and (c) z directions generated from an elliptical-shaped ferromagnets. The magnetization points to the $+y$ direction. Those fields generated from a stadium-shaped ferromagnets are shown in (d), (e), and (f).

frustration. In addition, the stadium-shaped ferromagnet sometimes includes vortices at the edges, depending on the size, and breaks the macrospin assumption [30, 31]. It results in a disappearance of magnetic pole, which is a topological charge in a spin ice [40] and plays a central role in frustration. This is another reason preferring the elliptical-shaped ferromagnet, rather than the stadium-shaped ferromagnet, applied to an artificial spin ice. The stadium-shaped ferromagnet might be, however, of use to different purposes, such as reservoir computing utilizing a ferromagnetic ensemble [41–43], where an external magnetic field is applied to the direction deviated from the easy (x) axis direction. In such a case, the stray magnetic field, pointing in a direction different from the

x -axis, may be generated and determines the magnetization alignment of the other ferromagnets. Then, the history of the applied field can be recognized from the magnetization alignment. The shape of the ferromagnet should be designed, depending on the purpose, and large-scale simulations, as well as experiments, will be necessary in future.

V. CONCLUSION

In summary, the stray magnetic fields generated from an elliptical-shaped and stadium-shaped ferromagnets were evaluated from the integral forms of the solutions

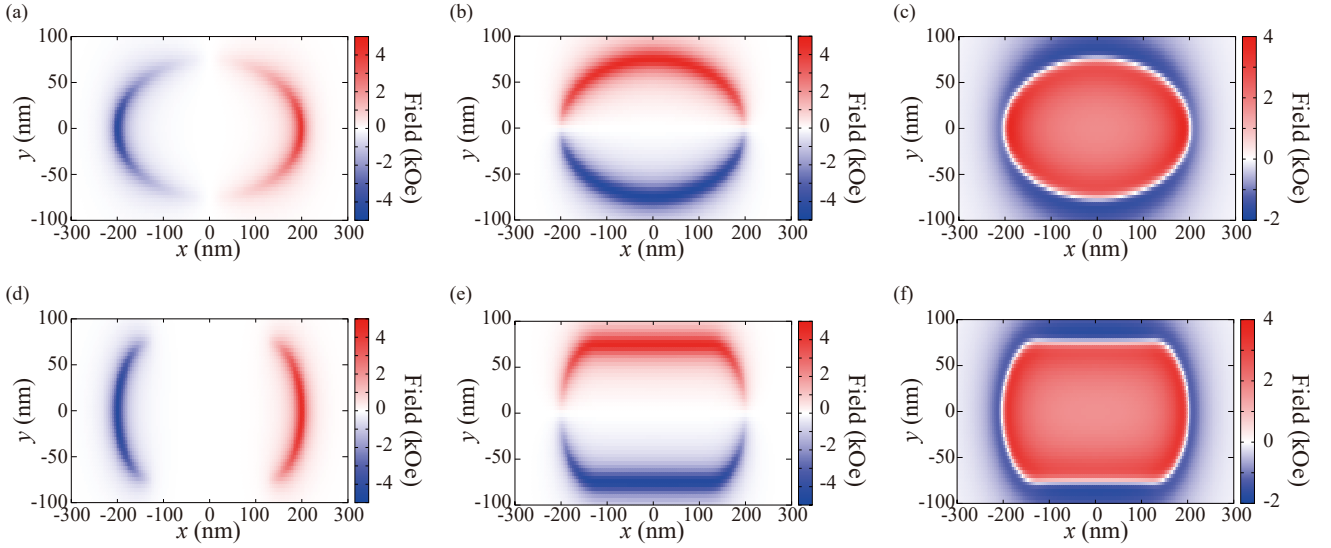


FIG. 6. (Color online) Stray fields in (a) x , (b) y , and (c) z directions generated from an elliptical-shaped ferromagnets. The magnetization points to the $+z$ direction. Those fields generated from a stadium-shaped ferromagnets are shown in (d), (e), and (f).

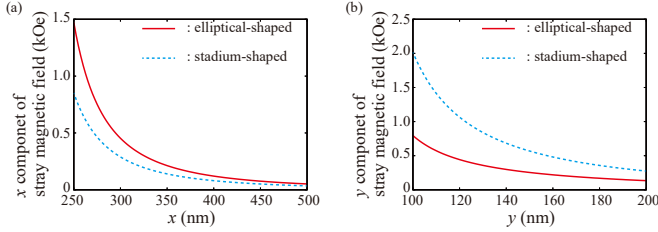


FIG. 7. (Color online) (a) The x components of the stray magnetic fields generated from the elliptical-shaped (red-solid) and the stadium-shaped (blue-dotted) ferromagnets, where the magnetization points to the $+x$ direction. The measurement points locate at $y = z = 0$. (b) The y components of the stray magnetic fields generated from the elliptical-shaped (solid red) and the stadium-shaped (dotted blue) ferromagnets, where the magnetization points to the $+y$ direction. The measurement points locate at $x = z = 0$.

of the Poisson equation. The results here will be useful for the estimation of the stray magnetic field with low calculation cost, as well as relatively high reliability than a point-particle approximation [43]. The elliptical-shaped ferromagnet generates a larger stray field than the stadium-shaped ferromagnet, when the magnetization points to the easy (long) axis direction. This is due to a larger density of the magnetic pole concentrated near the sample edge. The stadium-shaped ferromagnet, on the other hand, generates a larger stray magnetic field than the elliptical-shaped ferromagnet along the in-plane hard (short) axis direction because of the large number of the magnetic pole generated on the boundary. Regarding these results, the elliptical-shaped ferromagnet will be suitable when used in, for example, an artificial spin ice utilizing a large number of degenerated ground state. This is because, in such a system, the stray magnetic field generated by the magnetization which is ap-

proximately parallel to the easy axis causes a frustration and provides functionalities for multibit memory and so on. The stadium-shaped ferromagnet might be, on the other hand, of interest for reservoir computing utilizing ferromagnetic ensemble. This is because the magnetization direction is forcibly deviated from the easy axis by an external magnetic field, and thus, the stray magnetic field pointing in an arbitrary direction affects the magnetization alignment of the other ferromagnets.

ACKNOWLEDGEMENT

The author is grateful to Takehiko Yorozu for his enormous contribution to this work. The author is also thankful to Hitoshi Kubota for discussion. This work was supported by a JSPS KAKENHI Grant, Number 20H05655.

Appendix A: Verification of macrospin assumption

The applicability of the macrospin assumption was studied by performing micromagnetic simulation with MuMax3 [22]. The elliptical-shaped ferromagnet with $a = 200$ nm, $b = 75$ nm, and $h = 20$ nm was used for this purpose. The mesh number is 200, 75, and 10 in the x , y , and z direction, respectively, where we remind that the sample length (width) in the x (y) direction is $2a$ ($2b$), and thus, the mesh scale is 2 nm in every direction. The exchange stiffness is assumed to be 1.3×10^{-6} erg/cm.

Figure 8(a) shows the magnetization alignment after relaxation, where the initial state of the magnetization was set to be uniform in the x direction. An external magnetic field is absence in this example. In this case, even after the relaxation, the magnetization ap-

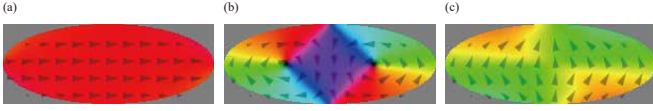


FIG. 8. (Color online) Magnetization alignment of an elliptical-shaped ferromagnet, in the absence of an external magnetic field, when the initial state is parallel to (a) x and (b) y axis. (c) Magnetization alignment in the presence of an external magnetic field of 1.0 kOe in the y direction, where the initial state is parallel to the y axis.

proximately points to the x direction uniformly. When the initial state was set to be uniform in the y direction, on the other hand, the magnetization alignment after relaxation becomes nonuniform, as schematically shown in Fig. 8(b). In this case, the magnetization state is energetically unstable, and the magnetic moments start to

change their direction to minimize the magnetic energy. The magnetization moments near the edge try to change their direction along the tangent of the ferromagnet, and as a result, magnetic vortices appear. In this case, the macrospin assumption does not work well. The magnetic vortices will also appear near the edges of the stadium-shaped ferromagnet due to its circular shape [30, 31]. When an external magnetic field is applied in the y direction, however, a uniform alignment of the magnetization is approximately recovered, as shown in Fig. 8(c), where the initial state was uniform to the y direction and the magnitude of the external magnetic field is 1.0 kOe. Note that, for $a = 200$ nm, $b = 75$ nm, and $h = 20$ nm, the demagnetization coefficients [9] are $N_x = 0.0406 \dots$, $N_y = 0.1549 \dots$, and $N_z = 0.8045 \dots$, and thus, the in-plane magnetic anisotropy field with $M = 1500$ is $4\pi M(N_y - N_x) = 2.153$ kOe.

-
- [1] J. A. Osborn, Demagnetizing Factors of the General Ellipsoid, *Phys. Rev.* **67**, 351 (1945).
 - [2] R. I. Joseph and E. Schlömann, Demagnetizing Field in Nonellipsoidal Bodies, *J. Appl. Phys.* **36**, 1579 (1965).
 - [3] R. I. Joseph, Ballistic Demagnetizing Factor in Uniformly Magnetized Cylinders, *J. Appl. Phys.* **37**, 4639 (1966).
 - [4] W. F. Druyvesteyn and J. W. F. Dorleijn, Calculations on some periodic magnetic domain structures: consequences for bubble devices, *Philips Res. Rep.* **26**, 11 (1971).
 - [5] D.-X. Chen, J. A. Brug, and R. B. Goldfarb, Demagnetizing Factors for Cylinders, *IEEE Trans. Magn.* **27**, 3601 (1991).
 - [6] A. Aharoni, Demagnetization factors for rectangular ferromagnetic prism, *J. Appl. Phys.* **83**, 3432 (1998).
 - [7] K. Y. Guslienko, Magnetostatic interdot coupling in two-dimensional magnetic dot arrays, *Appl. Phys. Lett.* **75**, 394 (1999).
 - [8] S. Tandon, B. Beleggia, Y. Zhu, and M. D. Graef, On the computation of the demagnetization tensor for uniformly magnetized particles of arbitrary shape. Part I: Analytical approach, *J. Magn. Magn. Mater.* **271**, 9 (2003).
 - [9] M. Beleggia, M. de Graef, Y. T. Millev, D. A. Goode, and G. Rowlands, Demagnetization factors for elliptic cylinders, *J. Phys. D: Appl. Phys.* **38**, 3333 (2005).
 - [10] M. Beleggia, M. de Graef, and Y. T. Millev, The equivalent ellipsoid of a magnetized body, *J. Phys. D: Appl. Phys.* **39**, 891 (2006).
 - [11] O. V. Sukhostavets, J. Gonzalez, and K. Y. Guslienko, Multiple magnetostatic interactions and collective vortex excitations in dot pairs, chains, and two-dimensional arrays, *Phys. Rev. B* **87**, 094402 (2013).
 - [12] K. Metlov, Vortex precession frequency and its amplitude-dependent shift in cylindrical nanomagnets, *J. Appl. Phys.* **114**, 223908 (2013).
 - [13] T. Taniguchi, Indirect excitation of self-oscillation in perpendicular ferromagnet by spin Hall effect, *Appl. Phys. Lett.* **111**, 022410 (2017).
 - [14] T. Taniguchi, An analytical computation of magnetic field generated from a cylinder ferromagnet, *J. Magn. Magn. Mater.* **452**, 464 (2018).
 - [15] A. Caciagli, R. J. Baars, A. P. Philipse, and B. W. M. Kuipers, Exact expression for the magnetic field of a finite cylinder with arbitrary uniform magnetization, *J. Magn. Magn. Mater.* **456**, 423 (2018).
 - [16] D. Mancilla-Almonacid, R. E. Arias, R. A. Escobar, D. Altbir, and S. Allende, Spin wave modes of two magnetostatic coupled spin transfer torque nano-oscillators, *J. Appl. Phys.* **124**, 162102 (2018).
 - [17] F. Slanovc, M. Ortner, M. Moridi, C. Abert, and D. Suess, Full analytical solution for the magnetic field of uniformly magnetized cylinder tiles, *J. Magn. Magn. Mater.* **559**, 169482 (2022).
 - [18] F. Masiero and E. Sinibaldi, Exact and Computationally Robust Solutions for Cylindrical Magnets Systems with Programmable Magnetization, *Adv. Sci.* **10**, 2301033 (2023).
 - [19] Y. Nakatani, Y. Uesaka, and N. Hayashi, Direct Solution of the Landau-Lifshitz-Gilbert Equation for Micromagnetics, *Jpn. J. Appl. Phys.* **28**, 2485 (1989).
 - [20] T. Komine, Y. Mitsui, and K. Shiiki, Micromagnetics of soft magnetic thin films in presence of defects, *J. Appl. Phys.* **78**, 7220 (1995).
 - [21] J. Ohe, S. E. Barnes, H.-W. Lee, and S. Maekawa, Electrical measurements of the polarization in a moving magnetic vortex, *Appl. Phys. Lett.* **95**, 123110 (2009).
 - [22] A. Vansteenkiste, J. Leliaert, M. Dvornik, M. Helsen, F. Garcia-Sanchez, and B. van Waeyenberge, The design and verification of MuMax3, *AIP Adv.* **4**, 107133 (2014).
 - [23] H. Tsukahara, S.-J. Lee, K. Iwano, N. Inami, T. Ishikawa, C. Mitsumata, H. Yanagihara, E. Kita, and K. Ono, Large-scale micromagnetics simulations with dipolar interaction using all-to-all communications, *AIP Adv.* **6**, 056405 (2016).
 - [24] C. Yoshida, H. Noshiro, Y. Yamazaki, T. Sugii, T. Tanaka, A. Furuya, and Y. Uehara, Micromagnetic simulation of electric-field-assisted magnetization switching in perpendicular magnetic tunnel junction, *AIP Adv.* **7**, 055935 (2017).
 - [25] F. A. Araujo, A. D. Belanovsky, P. N. Skirdkov, K. A. Zvezdin, A. K. Zvezdin, N. Loatelli, R. Lebrun, J. Grollier, and V. Cros, Optimizing magnetodipolar interac-

- tions for synchronizing vortex based spin-torque nano-oscillators, *Phys. Rev. B* **92**, 045419 (2015).
- [26] T. Taniguchi, Synchronized, periodic, and chaotic dynamics in spin torque oscillator with two free layers, *J. Magn. Magn. Mater.* **483**, 281 (2019).
 - [27] K. Y. Camsari, M. M. Torunbalci, W. A. Borders, H. Ohno, and S. Fukami, Double-Free-Layer Magnetic Tunnel Junctions for Probabilistic Bits, *Phys. Rev. Applied* **15**, 044049 (2021).
 - [28] M. A. Castro, D. Mancilla-Almonacid, B. Dieny, S. Alende, L. D. Buda-Prejbeanu, and U. Ebels, Mutual synchronization of spin-torque oscillators within a ring array, *Sci. Rep.* **12**, 12030 (2022).
 - [29] T. Yamaguchi, S. Tsunegi, K. Nakajima, and T. Taniguchi, Computational capability for physical reservoir computing using a spin-torque oscillator with two free layers, *Phys. Rev. B* **107**, 054406 (2023).
 - [30] H. Kubota *et al.*, presented at International Magnetic Conference (Intermag) 2023.
 - [31] H. Kubota *et al.*, accepted to IEEE Trans. Magn., 10.1109/TMAG.2023.3291380.
 - [32] R. F. Wang, C. Nisoli, R. S. Freitas, J. Li, W. McConville, B. J. Cooley, M. S. Lund, N. Samarth, C. Leighton, V. H. Crespi, and P. Schiffer, Artificial spin ice in a geometrically frustrated lattice of nanoscale ferromagnetic islands, *Nature* **439**, 303 (2006).
 - [33] M. Tanaka, E. Saitoh, H. Miyajima, T. Yamaoka, and Y. Iye, Magnetic interactions in a ferromagnetic honeycomb nanoscale network, *Phys. Rev. B* **73**, 052411 (2006).
 - [34] Y. Qi, T. Brintlinger, and J. Cumings, Direct observation of the ice rule in an artificial kagome spin ice, *Phys. Rev. B* **77**, 094418 (2008).
 - [35] E. Mengotti, L. J. Heyderman, A. F. Rodriguez, A. Bisig, L. L. Guyader, F. Nolting, and H. B. Braun, Building blocks of an artificial kagome spin ice: Photoemission electron microscopy of arrays of ferromagnetic islands, *Phys. Rev. B* **78**, 144402 (2008).
 - [36] A. Farhan, P. M. Derlet, A. Kleibert, A. Balan, R. V. Chopdekar, M. Wyss, L. Anghinolfi, F. Nolting, and L. J. Heyderman, Exploring hyper-cubic energy landscapes in thermally active finite artificial spin-ice systems, *Nat. Phys.* **9**, 375 (2013).
 - [37] A. Farhan, A. Kleibert, P. M. Derlet, L. Anghinolfi, A. Balan, R. V. Chopdekar, M. Wyss, S. Gliga, F. Nolting, and L. J. Heyderman, Thermally induced magnetic relaxation in building blocks of artificial kagome spin ice, *Phys. Rev. B* **89**, 214405 (2014).
 - [38] J. C. Gartside, D. M. Arroo, D. M. Burn, V. L. Bemer, A. Moskalenko, L. F. Cohen, and W. R. Brandford, Realization of ground state in artificial kagome spin ice via topological defect-driven magnetic writing, *Nat. Nanotechnol.* **13**, 53 (2018).
 - [39] S. T. Bramwell and M. J. Harris, The history of spin ice, *J. Phys.: Condens. Matter.* **32**, 374010 (2020).
 - [40] S. H. Skjærvø, C. H. Marrows, R. L. Stamps, and L. J. Heyderman, Advances in artificial spin ice, *Nat. Rev. Phys.* **2**, 13 (2020).
 - [41] J. C. Gartside, K. D. Stenning, A. Vanstone, H. H. Holder, D. M. Arroo, T. Dion, F. Carvavelli, H. Kurebayashi, and W. R. Brandford, Reconfigurable training and reservoir computing in an artificial spin-vortex ice via spin-wave fingerprinting, *Nat. Nanotechnol.* **17**, 460 (2022).
 - [42] W. Hu, Z. Zhang, Y. Liao, Q. Li, Y. Shi, H. Zhang, X. Zhang, C. Niu, Y. Wu, W. Yu, X. Zhou, H. Guo, W. Wang, J. Xiao, L. Yin, Q. Liu, and J. Shen, Distinguishing artificial spin ice states using magnetoresistance effect for neuromorphic computing, *Nat. Commun.* **14**, 2562 (2023).
 - [43] K. Hon, Y. Kuwabiraki, M. Goto, R. Nakatani, Y. Suzuki, and H. Nomura, Numerical simulation of artificial spin ice for reservoir computing, *Appl. Phys. Express* **14**, 033001 (2021).